06,04

Structure, microstructure, dielectric and piezoelectric properties of solid solution ceramics of a six-component system $(1\text{-}y\text{-}a\text{-}z)(Na_{0.5}K_{0.5}NbO_3)-yLiNbO_3-a/2CdNb_2O_6-zPb(Zr_{0.5}Ti_{0.5})O_3$

© K.P. Andryushin[1,2], E.V. Glazunova[1], L.A. Shilkina[1], A.V. Nagaenko[3], S.I. Dudkina[1], I.N. Andryushina[1], S.V. Khasbulatov[2,4], L.A. Reznichenko[1]

[1] Southern Federal University, Research Institute of Physics, Rostov-on-Don, Russia
[2] Kh. Ibragimov Complex Institute of the Russian Academy of Sciences, Groznyi, Russia
[3] Southern Federal University, Institute of High Technology and Piezo Technology, Rostov-on-Don, Russia
[4] A.A. Kadyrov Chechen State University, Institute of Mathematics, Physics and Information Technology, Groznyi, Russia

E-mail: kpandryushin@gmail.com

Received April 19, 2024
Revised April 19, 2024
Accepted April 24, 2024

For the first time, solid solutions of two sections of a six-component system KNN-LN-PZT-$CdNbO_6$ of the form $(1\text{-}y\text{-}a\text{-}z)(Na_{0.5}K_{0.5}NbO_3)-yLiNbO_3-a/2CdNb_2O_6-zPb(Zr_{0.5}Ti_{0.5})O_3$: were prepared by two-stage solid-phase synthesis followed by sintering using conventional ceramic technology: section I with $y = 0.05$, $a = 0.025$, $0.15 \le z < 0.50$; section II with $y = 0.10$, $a = 0.050$, $0.15 \le z < 0.50$. X-ray diffraction revealed that all the studied experimental samples have pseudocubic symmetry. The microstructure of ceramic solid solutions is characterized by extreme inhomogeneity. An analysis of the dielectric, piezoelectric, and elastic properties (macroresponses) of the experimental samples allowed for the identification of a group of compositions with high relative permittivity values, which are promising for low-frequency applications. A conclusion is made about the feasibility of utilizing the proposed compositions in the design of electronic devices.

Keywords: lead-free, $(Na,K)NbO_3$, $CdNb_2O_6$, $LiNbO_3$, ceramic.

DOI: 10.61011/PSS.2024.05.58502.95

1. Introduction

Transition to complex multicomponent systems (MS) is the main trend of the modern smart, primarily, electrically-active piezo materials science [1–5]. This is due to the fact that simpler compositions have achieved some saturation area in terms of properties that do not contribute to their already existing range as well as that the existing basic chemistry and design methods have been almost completely exhausted. Moreover, failure to implement a wide variety of options in mono, binary and ternary systems forces switching to MS where the benefits of each of the components are not only (and not so much) combined, but also a synergistic effect occurs in the atomic-molecular design process. As the number of components grows, the ranges of compounds with the best combinations of properties for various applications are extended, variety of properties increases suggesting considerable advantages of MS over their simpler components [6,7].

However, with an apparent huge potential of this research and development area, its development is restrained by the fact that the concepts of processes flowing in such complex systems resulting in formation of a targeted set of macro responses are understudied. To a certain extent, this presentation will try to fill this gap using a six-component system, including base compounds such as sodium, potassium, lithium, cadmium niobates and plumbum zirconate-titanate (PZT), in particular, containing non-isostructural components ($NaNbO_3$, $KNbO_3$, $PbTiO_3-ZrTiO_3$ — representative of the perovskite type family, $LiNbO_3$ — pseudo-ilmenite, $CdNb_2O_6$ — columbite [8–11]) that ensure novelty of physical properties of solid solutions (SS) in which they are involved [12,13]. While for binary systems $Pb(Ti,Zr)O_3$ and $(Na,K)NbO_3$, there is much of the literature since their discovery and till now (see, for example, [1,14–18]), there are very few published studies describing $(Na,K,Li)NbO_3$, $(Na,K)NbO_3-Pb(Ti,Zr)O_3$, $(Na,K)NbO_3-CdNb_2O_6$ systems [19–21].

2. Objects of research, preparation and test methods

The objects of research included KNN–LN–PZT–$CdNbO_6$ SS of type $(1\text{-}y\text{-}a\text{-}z)(Na_{0.5}K_{0.5}NbO_3)-yLiNbO_3-a/2CdNb_2O_6-zPb(Zr_{0.5}Ti_{0.5})O_3$: section I with

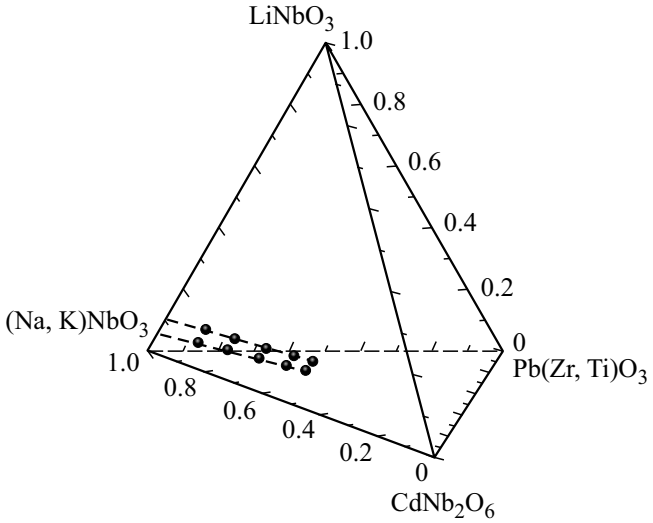

Figure 1. Tetrahedron of system compounds $(1\text{-}y\text{-}a\text{-}z)(Na_{0.5}K_{0.5}NbO_3)$–$y\,LiNbO_3$–$a/2CdNb_2O_6$–$z\,Pb(Zr_{0.5}Ti_{0.5})O_3$ with highlighted sections (dashed) and plotted experimental points.

$y = 0.05$, $a = 0.025$, $0.15 \le z < 0.50$; section II with $y = 0.10$, $a = 0.050$, $0.15 \le z < 0.50$.

Figure 1 shows a tetrahedron of compounds with highlighted sections of the six-component system (dashed) and experimental points. The samples were prepared by two-stage solid-phase synthesis followed by sintering using a conventional ceramic technique. The best sampling conditions were defined by varying process variables on a set of samples: $T_{synt.1} = 1220\,K$, $\tau_{synt.1} = 4\,h$, $T_{synt.2} = 1240\,K$, $\tau_{synt.2} = 4\,h$, $T_{sint.} = 1410-1470\,K$, $\tau_{sint.} = 2\,h$, depending on the compound. Section I samples with $z = 0.50$ and 0.15 were sintered without mechanical activation, samples with $z = 0.45$, 0.35, 0.25 underwent double mechanical activation: for the charge and synthesized products before sintering. In section II, all samples underwent double mechanical activation. Mechanical activation (high-energy milling in AGO-2 drums, speed — 1800 rpm) was performed in a ball planetary mill during 15 min. The samples with $z = 0.50$ and 0.15 were sintered without mechanical activation, the samples with $z = 0.45$, 0.35, 0.25 underwent double mechanical activation in the ball planetary mill during 15 min (high-energy milling in AGO-2 drums, speed — 1800 rpm. Sintered ceramic workpieces were machined (cut in plane, ground and polished on flat surfaces and ends) to make $\varnothing 10 \times 1$ mm measurement samples. Each set of such samples included 8–10 pieces. Before metallization, the samples were baked at $T_{anneal.} = 770\,K$ during 0.5 h to remove residual organic substances and degrease the surfaces to improve adhesion between the metallic coating and ceramic. Electrodes were applied by baking silver-containing paste into the flat surfaces of the sample at 1070 K during 0.5 h.

X-ray tests were performed by the powder diffraction method using DRON-3 diffractometer (CoKα-radiation) with mounted IR-2 X-ray ratemeter. powdered ceramic items were examined to avoid the influence of surface effects, stresses and textures occurring during the ceramic preparation process. Structural parameters were calculated using standard procedures [22]. Structural parameter measurement errors were as follows: linear $\Delta a = \Delta b = \Delta c = \pm(0.002-0.004)$ Å; angular $\Delta\beta = 3'$; volume $\Delta V = \pm 0.05$ Å^3 ($\Delta V/V \cdot 100\% = 0.07\%$). Modulation parameters, wave number k and modulation wavelength Λ were calculated using equations $k = |1/d_{hkl} - 1/d_s|$, $\Lambda = k^{-1}$, where d_{hkl} and d_s are interplanar spacings of the diffraction peak and satellite, respectively [22].

Grain structure of the objects were examined using JSM-6390L (Japan) scanning election microscope with Oxford Instruments (UK) microanalyzer system. Microscope resolution — up to 1.2 nm at an accelerating voltage of 30 kV (secondary electron image), accelerating voltage limits — from 0.5 to 30 kV, increase from $\times 10$ to $\times 1000000$, beam current up to 200 nA.

Electrophysical properties of SS were measured at room temperature ($T = 300\,K$) using Agilent 4980A LCR-meter by the resonance-antiresonance method [23], relative permittivities of nonpolarized ($\varepsilon'/\varepsilon_0$) and polarized ($\varepsilon^T_{33}/\varepsilon_0$) samples, low-field dielectric loss (dielectric loss angle tangent, $\mathrm{tg}\,\delta$), piezoelectric constants (d_{ij}: $|d_{31}|$, d_{33}), piezoelectric coefficient (piezosensitivities) (g_{ij}: $|g_{31}|$, g_{33}), electromechanical coupling coefficients of planar oscillation mode (K_p), mechanical Q factor (Q_m), Young's modulus (Y^E_{11}), speed of sound (V^E_1) were measured. Electrophysical measurement errors are as follows: $\varepsilon/\varepsilon_0$, $\varepsilon^T_{33}/\varepsilon_0 \le \pm 1.5\%$, $K_p \le \pm 2.0\%$, $|d_{31}| \le \pm 4.0\%$, $d_{33} \le \pm 10\%$, $Q_m = \le \pm 12\%$; $Y_{11} \le \pm 0.7\%$. piezoelectric constant d_{33} and, respectively, piezoelectric coefficient g_{33} were examined at room temperature by the quasistatic method using Piezo d_{33} Test System (YE2730A d_{33} METER).

Dependences of the real ($\varepsilon'/\varepsilon_0$) and imaginary ($\varepsilon''/\varepsilon_0$) parts of the relative complex permittivity $\varepsilon^*/\varepsilon_0 = \varepsilon'/\varepsilon_0 - i\varepsilon''/\varepsilon_0$ ($\varepsilon_0 = 8.75 \cdot 10^{-12}$ F/m — dielectric constant) on the nonpolarized sample temperature at $T = (300 - 900)\,K$ within $f = (25-10^6)$ Hz were measured using a measurement bench on the basis of Agilent 4980A LCR-meter.

3. Experimental findings and discussion

Figure 2 shows X-ray images of section I solid solutions where it can be seen that all samples were crystallized in the perovskite type structure without foreign phases, only two samples with high PZT concentration contain a low amount of pyrochlore phase and ZrO_2.

X-ray images of solid solutions have the following features: diffraction peak bases are broadened, superstructural reflections indicating perovskite cell multiplication are absent, peak splitting in one sample does not correspond to

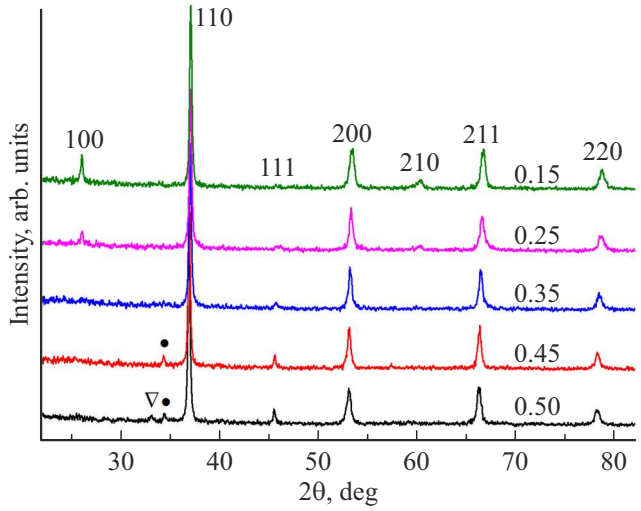

Figure 2. X-ray images of SS $(1-y-a-z)$ $(Na_{0.5}K_{0.5}NbO_3)$–$y LiNbO_3 - a/2 CdNb_2O_6 - z Pb(Zr_{0.5}Ti_{0.5})O_3$ with $y = 0.05$, $a = 0.025$ (black circle shows the pyrochlore lines, triangle shows ZrO_2 line, numbers on the right hand show PZT concentration).

any distinct lattice symmetry. At the same time, at all values of z, there is splitting of diffraction peaks, that is particularly pronounced on peaks 200 and 211 (see Figure 3), therefore solid solution symmetry is denoted ans pseudocubic (Psc). Diffusion scattering transforms into satellite peaks near some diffraction peaks. Figure 3 illustrates diffraction peaks 200, 220 and 211 of solid solutions with $z = 0.15$, 0.35, 0.50. Occurrence of satellites indicates that the structure is in the modulated state. For the diffraction peaks shown in Figure 3, positions of their satellites were used to calculate the modulation wavelengths, λ.

In SS with $z = 0.15$ in $\langle 100 \rangle$ direction, calculated using satellites S_1^- and S_2^-, $\lambda_1 \approx 340$ Å, $\lambda_2 \approx 170$ Å, in SS with $z = 0.35$ in $\langle 110 \rangle$ direction $\lambda_1 \approx 644$ Å, $\lambda_2 \approx 322$ Å, in SS with $z = 0.50$ in $\langle 211 \rangle$ direction $\lambda_1 \approx 428$ Å, $\lambda_2 \approx 216$ Å. In all cases $\lambda_2 = 1/2\lambda_1$, the presence of even satellites is a sign of sinusoidal modulation specific to the concentration wave. This suggests that the samples are chemically inhomogeneous and contain at least two solid solutions with close cell parameters. Alternation frequency of regions having different chemical compositions results in modulation of the structure.

For calculation of the perovskite cell parameters, the diffraction peaks were approximated by the Lorentz function as single ones. Figure 4 shows the concentration dependences of the cell volume V, halfwidth B, diffraction peak 200 and ceramic sample density.

Increase in V may be due to the heterovalent substitution $Pb^{2+} \rightarrow A^{1+}$, where either A^{1+} vacancies are formed or interstitial anions occur. In both cases, solid solution lattice swelling takes place. Substitution $Pb^{2+} \leftrightarrow Cd^{2+}$ is also possible, however, it may be limited due to high difference in ionic radii (27% with allowable 15% for SS substitution [24]): $R(Pb^{2+}) = 1.26$, $R(Cd^{2+}) = 0.99$ at coordination number 6 according to Belov–Bokiy [25]. Wide valley on $B(z)$ and high density of ceramics within $0.25 \leq z \leq 0.45$ are explained by mechanical activation of these solid solutions that resulted in considerable increase in their homogeneity and density.

Figure 5 shows X-ray images of SS where none of SS's was formed without using impurity phases: ZrO_2 [26] and $Pb_3Nb_4O_{13}$ [27]. Like in section I, all samples are inhomogeneous in terms of chemical composition, as z grows, inhomogeneity increases, diffraction peaks are wide, peak bases are highly distorted by diffusion scattering.

Pyrochlore phase at $z = 0.25$ gas cubic symmetry with $a = 10.58$ Å, at $z = 0.5$ — $a = 10.537$ Å. JCPDS database shows cell parameters of $(Cd_{1-x}Pb_x)2Nb_2O_7$ SS for $x = 0.25$ [28], $x = 0.5$ [29] and $x = 0.9$ [30]. $a(x)$ curve plotted using these data with points corresponding to the pyrochlore cell parameters calculated herein is shown in Figure 6. It is shown that all points ideally fit the straight line and this suggests that the pyrochlore phase in the test samples is $(Cd_{1-x}Pb_x)_2Nb_2O_7$ SS whose compositions varies as z grows. Chemical formulas of SS with pyrochlore

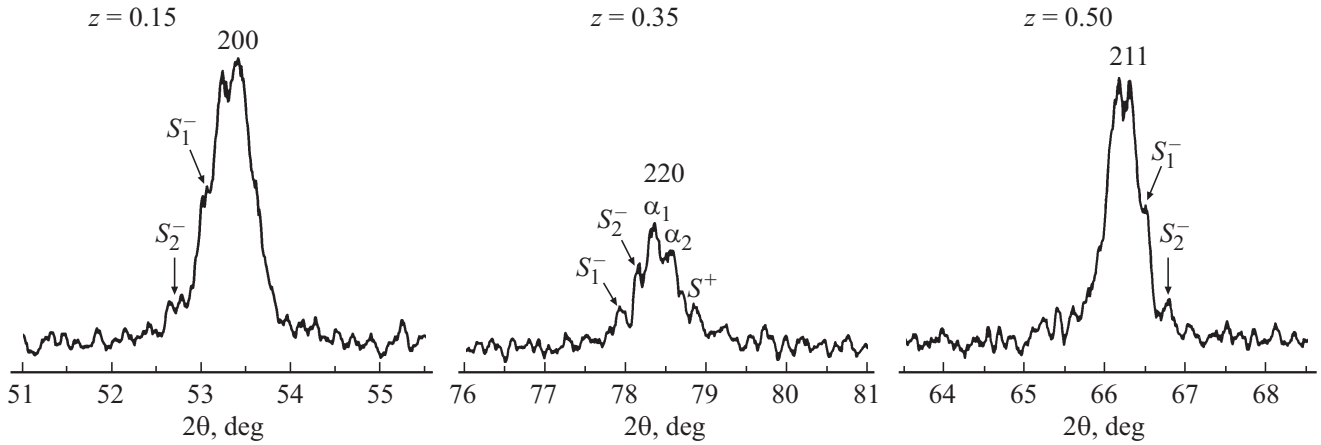

Figure 3. Diffraction peaks with satellites of solid solutions with $y = 0.05$, $a = 0.025$ at $z = 0.15$, 0.35, 0.50.

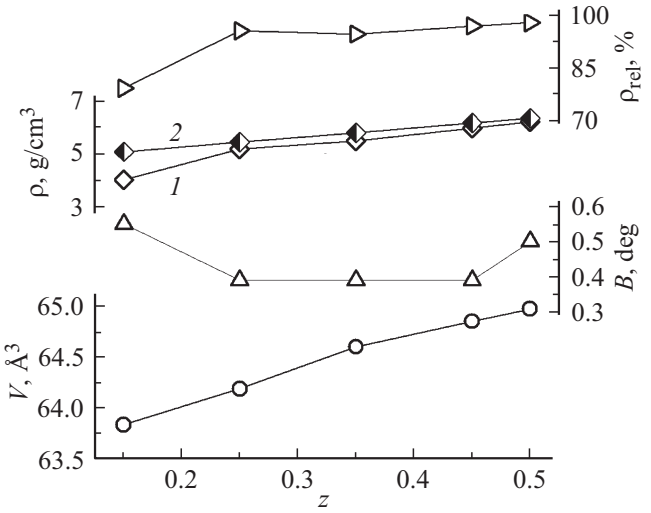

Figure 4. Dependences of cell volume V, X-ray peak halfwidth 200, B, experimental (curve *1*), X-ray (*2*) and relative densities of SS ceramics $(1\text{-}y\text{-}a\text{-}z)(Na_{0.5}K_{0.5}NbO_3)$–$y$LiNbO$_3$–a/2CdNb$_2O_6$–$zPb(Zr_{0.5}Ti_{0.5})O_3$ with $y = 0.05$, $a = 0.025$ on the PZT concentration (z).

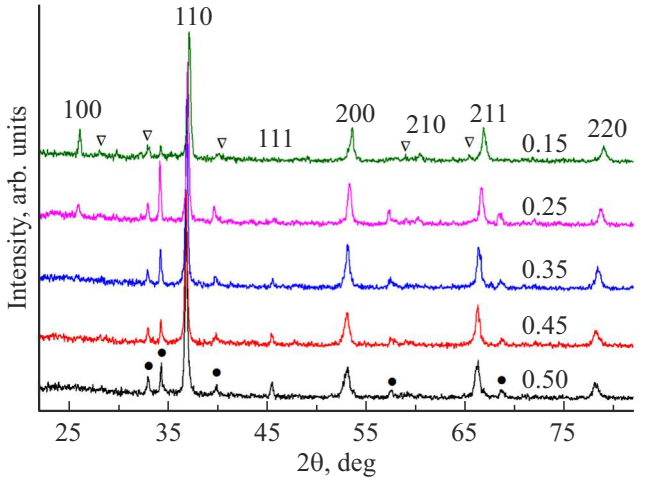

Figure 5. X-ray images SS $(1\text{-}y\text{-}a\text{-}z)(Na_{0.5}K_{0.5}NbO_3)$–$y$LiNbO$_3$–$a$/2CdNb$_2O_6$–$zPb(Zr_{0.5}Ti_{0.5})O_3$ with $y = 0.10$, $a = 0.050$ (black circle shows the pyrochlore lines, triangle shows ZrO_2 lines, numbers on the right hand show PZT concentration).

structure corresponding to the cell parameters are shown in the caption to Figure 6. It should be noted that as Pb concentration z grows in the samples, Pb content in the pyrochlore phase decreases, while Cd content increases, which indicates limited solubility of the latter in the given SS.

For calculation of the perovskite cell parameters, like in section 1, the diffraction peaks were approximated by the Lorentz function as single ones. Dependences of cell volume, X-ray peak halfwidth 200 and densities of section II SS ceramics on the PZT concentration z are shown in Figure 7. Due to high amount of pyrochlore in the composition of the samples, real Pb concentration in perovskite type SS may not correspond to z.

Increase in V within $0.15 \leq z \leq 0.35$ may be due, like in section I SS, to the heterovalent substitution $Pb^{2+} \rightarrow A^{1+}$, where either A^{1+} vacancies are formed or interstitial anions occur. In both cases, SS lattice swelling takes place. The curve shows that the whole concentration range is divided into two regions with an interface at $z = 0.35$. In region $z < 0.35$, Pb^{2+} in built in the SS lattice. At $z > 0.35$, SS inhomogeneity increases (B grows), Pb^{2+} introduction into

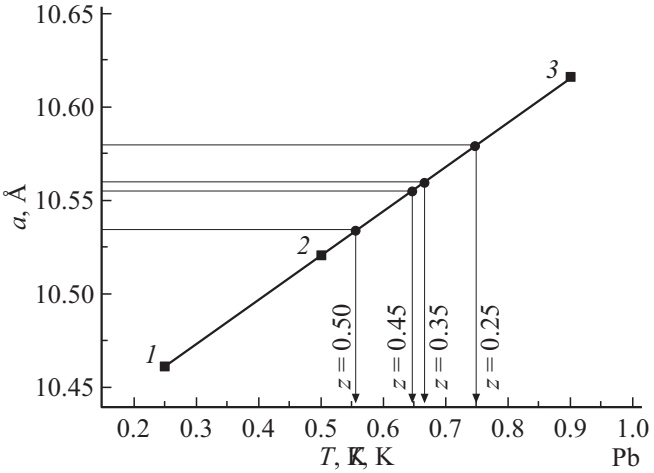

Figure 6. Dependence of cubic cell parameter of $(Cd_{1-x}Pb_x)2Nb_2O_7$ solid solution according to JCPDS data: point *1*, point *2*, point *3*. Circles show parameters calculated herein. Chemical formulas corresponding to the calculated cell parameters: $z = 0.25$ — $(Pb_{0.75}Cd_{0.25})_2Nb_2O_7$; $z = 0.35$ — $(Pb_{0.67}Cd_{0.33})_2Nb_2O_7$; $z = 0.45$ — $(Pb_{0.64}Cd_{0.36})_2Nb_2O_7$; $z = 0.50$ — $(Pb_{0.56}Cd_{0.44})2Nb_2O_7$.

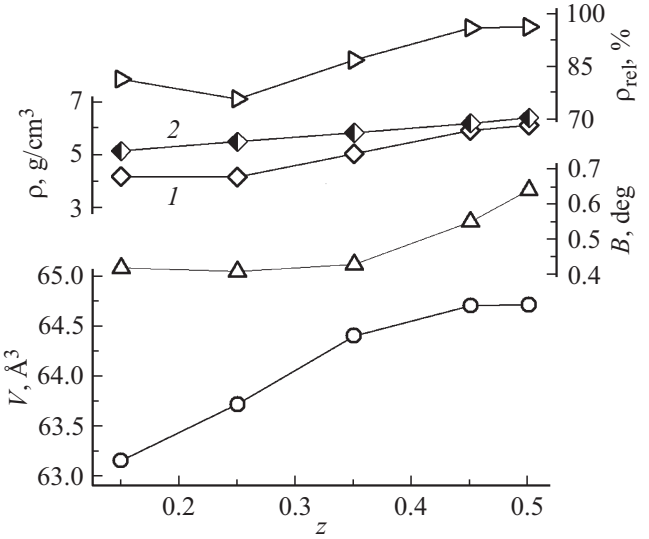

Figure 7. Dependences of cell volume V, X-ray peak halfwidth 200, B, experimental (curve *1*), X-ray (*2*) and relative densities of KNN–LN–PZT–CdNbO$_6$ SS ceramics with $y = 0.10$, $a = 0.050$ on PZT concentration (z).

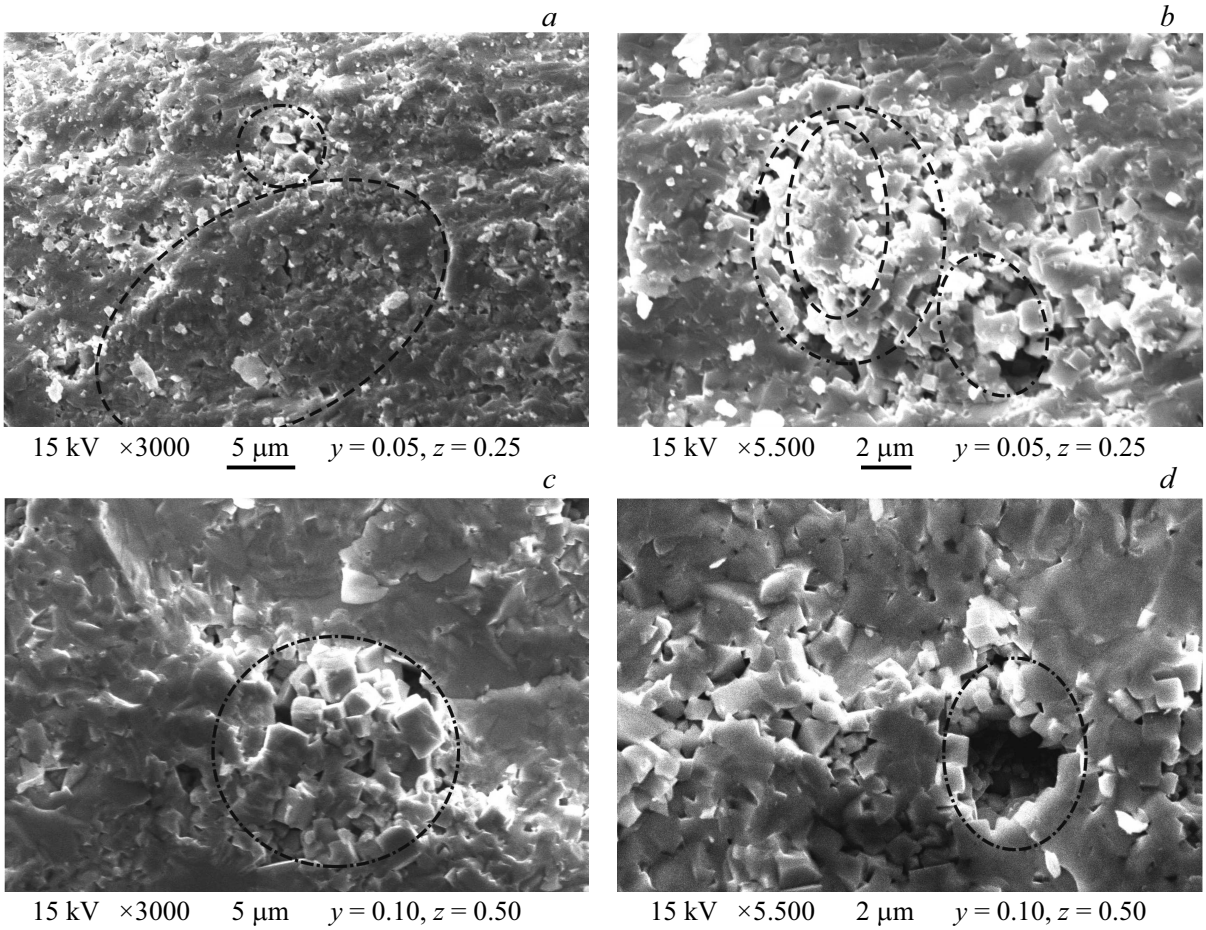

Figure 8. Fragments of SS ceramics $(1\text{-}y\text{-}a\text{-}z)(Na_{0.5}K_{0.5}NbO_3)-yLiNbO_3-a/2CdNb_2O_6-zPb(Zr_{0.5}Ti_{0.5})O_3$ *a*) $y = 0.05$, $a = 0.05$, $z = 0.25$; *b*) $y = 0.10$, $a = 0.10$, $z = 0.15$.

the SS lattice decreases and stops at $z \geq 0.45$, $V = \text{const}$. In SS inhomogeneity growing conditions, density, as it may seem strange,grows. This is due to the fact that, when an impurity phase is present, it is impossible to estimate the contribution of each of the phases to the sample density.

Microstructure of the taken ($y = 0.05$, $a = 0.05$, $z = 0.25$; $y = 0.10$, $a = 0.10$, $z = 0.15$) (Figure 8) $((1\text{-}y\text{-}a\text{-}z)(Na_{0.5}K_{0.5}NbO_3)-yLiNbO_3-a/2CdNb_2O_6-zPb(Zr_{0.5}Ti_{0.5})O_3)$ 6-component system samples, like, however, of all other examined sections I ($y = 0.05$, $a = 0.05$, $0.15 \leq z \leq 0.50$) and II ($y = 0.10$, $a = 0.10$, $0.15 \leq z \leq 0.50$) features outstanding inhomogeneity. However, in section I SS where the sample with $y = 0.05$, $a = 0.05$, $z = 0.25$ is localized, this is the inhomogeneity of grain packaging: there are regions with closely-packed crystallites (shown dashed in the figure), loose structures (shown dashed and dotted) and combining both types od grain contacts. In section II SS with $y = 0.10$, $a = 0.10$, $z = 0.15$, the system has dimensional inhomogeneity — two types of grains are crystallized: coarse grains in the form of parallelepipeds and fine grains in a near-cubic form. Such bimodal structures in some cases occur against the background of areas with loose grain packaging.

As has been mentioned many times, the described grain morphology is specific to recrystallization processes flowing with liquid phases. Non-reacted initial reagents or low-melting eutectics in charges of alkaline and alkaline earth metals, PZT, for example, Na_2O with $T_{melt.} = 1405\,K$; K_2O with $T_{melt.} = 1013\,K$; PbO with $T_{melt.} = 1160\,K$; CdO with $T_{melt.} = 1173\,K$; Na_2CO_3 with $T_{melt.} = 1127\,K$; K_2CO with $T_{melt.} = 1164\,K$; Li_2CO_3 with $T_{melt.} = 1005\,K$; $PbCO_3$ with $T_{melt.} = 588\,K$; NaOH with $T_{melt.} = 596\,K$; KOH with $T_{melt.} = 678\,K$; LiOH with $T_{melt.} = 735\,K$; $NaNbO_3$ with $T_{melt.} = 1695\,K$; $KNbO_3$ with $T_{melt.} = 1373\,K$, etc., may serve as sources.

It has been established that in all studied SS belonging to section I, in the area of transition to a nonpolar phase, smeared peaks of relative dielectric permittivity $\varepsilon'/\varepsilon_0$ are observed. They are reduced, diffused and shifted into a higher temperature area as the frequency grows, which is specific to ferroelectric relaxers (Figure 9). $\varepsilon'/\varepsilon_0$ shows similar behavior also in section II SS with $z > 0.25$. In SS belonging to section II with $z = 0.15$, formation of two peaks was detected on $\varepsilon'/\varepsilon_0$ at $T \approx 300$ and 525 K. the first peak has a form specific to traditional ferroelectric materials, the second peak is shifted into a lower temperature region

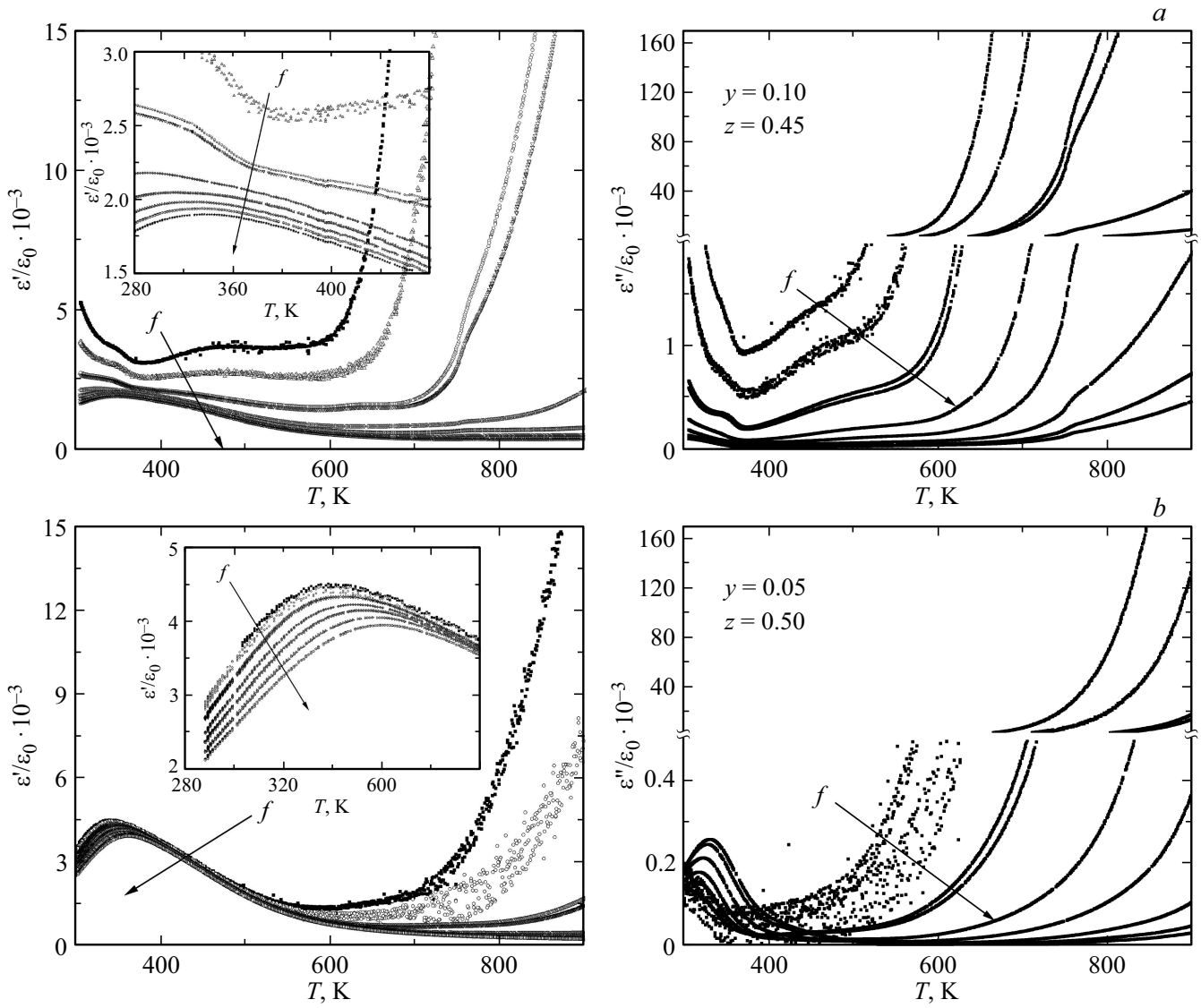

Figure 9. temperature dependences of real and imaginary parts of the relative permittivities of SS system $(1\text{-}y\text{-}a\text{-}z)(Na_{0.5}K_{0.5}NbO_3)-yLiNbO_3-a/2CdNb_2O_6-z\,Pb(Zr_{0.5}Ti_{0.5})O_3$ with $y = 0.05$, $a = 0.025$, $x = 0.475$, $0.15 \le z \le 0.5$ measured at $f = (20-2 \cdot 10^6)$ Hz.

as the frequency grows, which is probably due to the conductance effect. In SS with $z = 0.25$, there is a TC peak that is highly smeared in a wide temperature range and is not shifted in temperature as f varies. Critical dependence of SS dielectric properties on elemental composition was also detected. Thus, in SS from section I, TC moves into a lower temperature region from ~ 470 to 330 K as the content of z increases from 0.15 to 0.35.

After achievement of the specified value, $z = 0.35$ TC grows by $(5-15)$ K. In section II, similar phenomena take place at z equal to $(0.15-0.35)$. In the PE region at $T > 600$ K all given SS show rapid growth of $\varepsilon'/\varepsilon_0$ that may be due to oxidation-reduction processes, associated with the mixed valence of Nb $^{(5+\leftrightarrow 4+)}$ and Ti$^{(4+\leftrightarrow 3+)}$ [31,32], that facilitate the appearance of oxygen vacancies and generate anion-deficient nonstoichiometry. Being weakly associated with material structure, these vacancies are the source of conductance and make additional contribution to the development of dielectric properties of SS.

Figure 10 shows (illustrated by section I) dielectric, piezoelectric and elastic properties (macroresponses) of SS depending on concentration z of $(Pb(Zr_{0.5}Ti_{0.5})O_3)$. It has been established that the given sections of the system have TC reduction with increasing concentration up to $z = 0.35$, interchanged with a minor rise. Difference in dielectric parameters $(\varepsilon/\varepsilon_0,\ \varepsilon_{33}^{\mathrm{T}}/\varepsilon_0,\ \mathrm{tg}\,\delta)$ shall be noted for two given section. Thus, in SS with $a = 0.05$ at $z = 0.15$, these properties are reduced significantly after formation of the polar state. Growth of PZT concentration $z > 0.15$ causes drop of $\Delta\varepsilon/\varepsilon$ to $\sim 500-800$. For SS with $a = 0.10$, decrease of $\Delta\varepsilon/\varepsilon$, $\varepsilon_{33}^{\mathrm{T}}/\varepsilon_0$, $\mathrm{tg}\,\delta$ in polar state is also specific, however, $\Delta\varepsilon/\varepsilon$ varies in smaller ranges. Thus, at $z = 0.15$

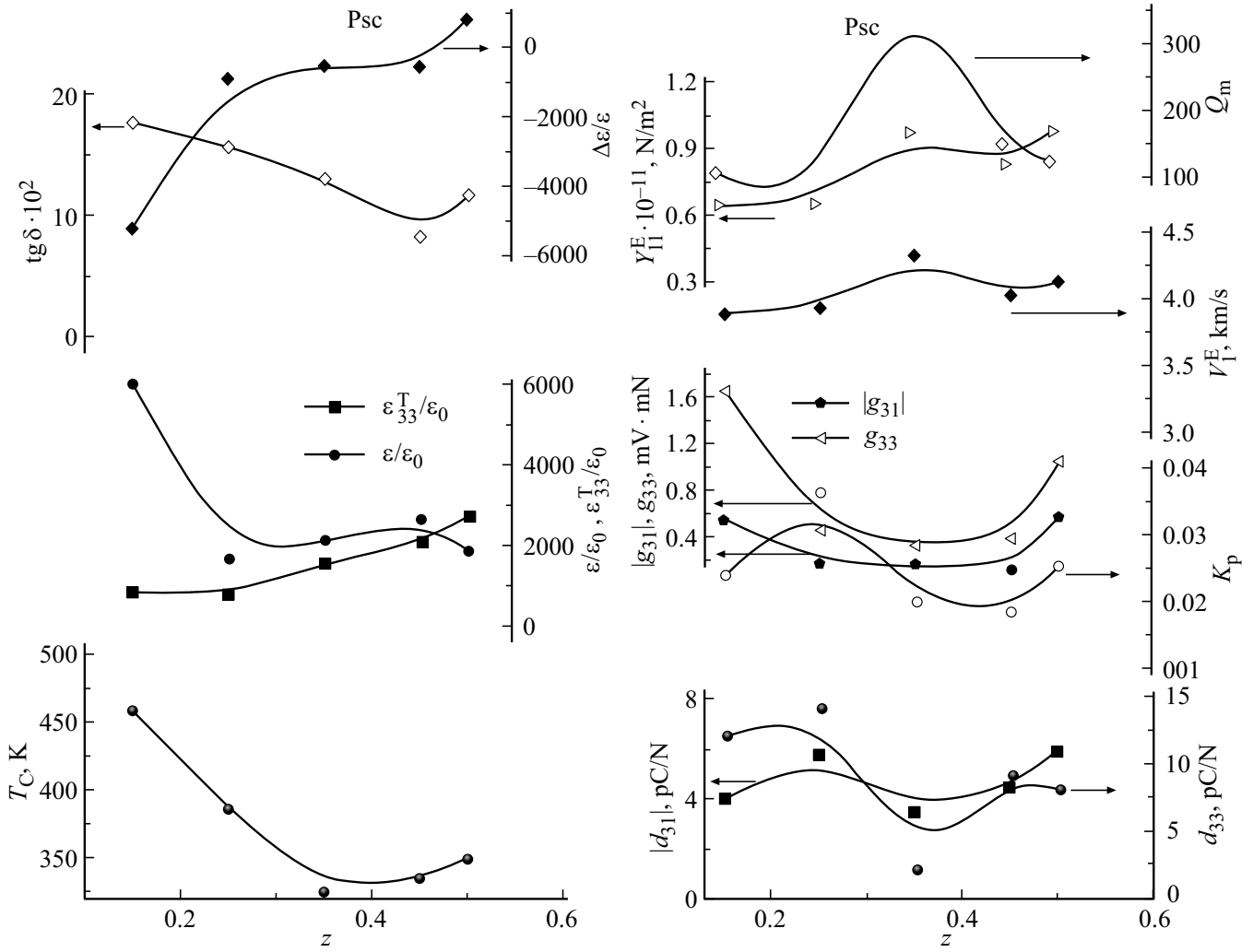

Figure 10. Dependences of dielectric, piezoelectric and elastic properties of SS $(1\text{-}y\text{-}a\text{-}z)(Na_{0.5}K_{0.5}NbO_3)$–$y LiNbO_3 - a/2CdNb_2O_6 - z Pb(Zr_{0.5}Ti_{0.5})O_3$ ($y = 0.05$, $a = 0.025$) ($T = 300$ K).

and 0.25, $\Delta\varepsilon/\varepsilon$ is 1000 and 470, respectively. At PZT concentration 35 mol.%, peak $\Delta\varepsilon/\varepsilon \approx 2000$ is observed, then $\Delta\varepsilon/\varepsilon$ decreases to ~ 400 and remains almost unchanged with growth of z. piezoelectric and elastic properties for the given SS sections demonstrate non-monotonic behavior as the peak is formed at $z \approx 0.35$. However, it should be noted that this anomaly is less pronounced in SS with $a = 0.10$. Formation of peaks on various curves of SS with $z = 0.30-0.40$ (Figure 10) may be due to the stabilization of the perovskite structure, growth of the relative density of the given samples and by possible local structural instabilities that occur when quite large amounts of PZT component are introduced and resulting elemental composition inhomogeneities occur in SS.

Analysis of the measured dependences made it possible to identify a group of compositions with high relative dielectric permittivities ($\varepsilon_{33}^{T}/\varepsilon_0 \approx 5000-6000$) that are promising for low-frequency applications and for various frequency filters.

4. Conclusion

For the first time, the two-stage solid-phase synthesis followed by sintering with a traditional ceramic technique (without externally applied pressure) was used to prepare ceramic solid solutions of two sections of six-component system $(1\text{-}y\text{-}a\text{-}z)(Na_{0.5}K_{0.5}NbO_3)-yLiNbO_3-a/2CdNb_2O_6-zPb(Zr_{0.5}Ti_{0.5})O_3$: section I with $y = 0.05$, $a = 0.025$, $0.15 \le z < 0.50$; section II with $y = 0.10$, $a = 0.050$, $0.15 \le z < 0.50$. Structural examination has shown that all given solid solutions have pseudocubic crystal system. It has been shown that the microstructure of ceramic solid solutions had an outstanding inhomogeneity. In all given SS from section I, behavior of $\varepsilon'/\varepsilon_0$ that is inherent in ferroelectric relaxers has been detected. $\varepsilon'/\varepsilon_0$ shows similar behavior also in section II SS with $z > 0.25$. Analysis of dielectric, piezoelectric and elastic properties (macroresponses) of the test samples identified a group of compositions with high relative

dielectric permittivities that are promising for low-frequency applications.

The obtained results shall be preferably used in the development of similar materials and electronic devices based on these materials.

Funding

The study was supported by the Ministry of Science and Higher Education of the Russian Federation (State assignment in the field of research. Project No. FENW-2023-0010/(GZ0110/23-11-IF). Equipment was provided by the Center for the Collective Use of Scientific Equipment of the Research Institute of Physics, Southern Federal University, „Electromagnetic, Electromechanical and Thermal Properties of Solid Bodies“.

Conflict of interest

The authors declare that they have no conflict of interest.

References

[1] B. Jaffe, W. Cook, H. Jaffe. Piezoelectric Ceramics. Academic Press, N.Y. (1971). 317 p.
[2] D. Berlincourt. Piezoelectric crystals and ceramics. In: Ultrasonic Transducer Materials: Piezoelectric Crystals and Ceramics / Ed. O.E. Mattiat. Plenum Press, London (1971). P. 63.
[3] L.A. Reznichenko, I.A. Verbenko, L.A. Shilkina, A.V. Pavlenko, S.I. Dudkina, I.N. Andryushina, K.P. Andryushin, A.G. Abubakarov, T.V. Krasnyakova. Springer Proceed. Phys. **207**, *3* (2018). https://doi.org/10.1007/978-3-319-78919-4_1
[4] C.C. Tsai, S.Y. Chu, C.K. Liang. J. Alloys Compd. **478**, *1–2*, 516 (2009). https://doi.org/10.1016/j.jallcom.2008.11.084
[5] A.V. Nagaenko, S.-H. Chang, K.P. Andryushin, L.A. Shilkina, M.I. Mazuritskiy, I.N. Andryushina, E.V. Glazunova, A.A. Pavelko, Y.A. Trusov, I.A. Verbenko, L.A. Reznichenko, I.A. Parinov. Heliyon **6**, e03497 (2020). https://doi.org/10.1016/j.heliyon.2020.e03497
[6] A.Y. Dantsiger, N.V. Dergunova, S.I. Dudkina, E.G. Fesenko. Ferroelectrics **132**, *1*, 213 (1992). https://doi.org/10.1080/00150199208009087
[7] L.A. Reznichenko, A.Y. Dantsiger, O.N. Razumovskaya, S.I. Dudkina, I.P. Raevskii, L.A. Shilkina, A.N. Klevtsov. Inorg. Mater. **37**, *12*, 1289 (2001). https://doi.org/10.1023/a:1012934327319
[8] A. Savage. J. Appl. Phys. **37**, *8*, 3071 (1966). https://doi.org/10.1063/1.1703164
[9] K. Chen, Y. Zhu, Z. Liu, D. Xue. Molecules **26**, *22*, 1 (2021). https://doi.org/10.3390/molecules26227044
[10] E. Aleshin, R. Roy. J. Am. Ceram. Soc. **45**, *1*, 18 (1962). https://doi.org/10.1111/j.1151-2916.1962.tb11022.x
[11] B. Lewis, E.A.D. White. J. Electron. Control **1**, *6*, 646 (1956). https://doi.org/10.1080/00207215608961468
[12] K.-I. Kakimoto, K. Akao, Y. Guo, H. Ohsato. Jpn. J. Appl. Phys. Part 1 Regul. Pap. Short Notes Rev. Pap. **44**, *9S*, 7064 (2005). https://doi.org/10.1143/JJAP.44.7064
[13] Y. Guo, K.I. Kakimoto, H. Ohsato. Appl. Phys. Lett. **85**, *18*, 4121 (2004). https://doi.org/10.1063/1.1813636
[14] P.K. Panda, B. Sahoo. Ferroelectrics **474**, *1*, 128 (2015). https://doi.org/10.1080/00150193.2015.997146
[15] M.-G. Kang, W.-S. Jung, C.-Y. Kang, S.-J. Yoon. Actuators **5**, *1*, 5 (2016). https://doi.org/10.3390/act5010005
[16] G.L. Smith, J.S. Pulskamp, L.M. Sanchez, D.M. Potrepka, R.M. Proie, T.G. Ivanov, R.Q. Rudy, W.D. Nothwang, S.S. Bedair, C.D. Meyer, R.G. Polcawich. J. Am. Ceram. Soc. **95**, *6*, 1777 (2012). https://doi.org/10.1111/j.1551-2916.2012.05155.x
[17] O. Tokay, M. Yazıcı. Mater. Today Commun. **31**, 103358 (2022). https://doi.org/10.1016/j.mtcomm.2022.103358
[18] J. Wu, D. Xiao, J. Zhu. Chem. Rev. **115**, *7*, 2559 (2015). https://doi.org/10.1021/cr5006809
[19] Q. Yin, S. Yuan, Q. Dong, C. Tian. J. Am. Ceram. Soc. **93**, *1*, 167 (2010). https://doi.org/10.1111/j.1551-2916.2009.03367.x
[20] K. Andryushin, L. Shilkina, I. Andryushina, A. Nagaenko, M. Moysa, S. Dudkina, L. Reznichenko. Mater. **14**, *14*, 4009 (2021). https://doi.org/10.3390/ma14144009
[21] K.P. Andryushin, L.A. Shilkina, I.N. Andryushina, M.O. Moysa, D.I. Rudsky, L.A. Reznichenko. Ceram. Int. **47**, *1*, 138 (2021). https://doi.org/10.1016/j.ceramint.2020.08.117
[22] A. Guinier. Théorie et Technique de la Radiocrystallographie, 2nd. ed. Dunod, Paris (1956) 736 p.
[23] IEEE Standard on Piezoelectricity ANSI/IEEE Std 176–1987, N.Y. (1988). https://doi.org/10.1109/IEEESTD.1988.79638
[24] V.S. Urusov. Theory of Isomorphic Miscibility. Nauka, M. (1977). 251 p.
[25] G.B. Bokiy. Vvedenie v kristallokhimiyu. Izd-vo MGU, M. (1954). 491 p. (in Russian).
[26] Powder Diffraction File. Data Cards. Inorganic Section. Set 37, card 1484. JCPDS, Swarthmore, PA, USA (1948).
[27] Powder Diffraction File. Data Cards. Inorganic Section. Set 25, card 443. JCPDS, Swarthmore, PA, USA (1948).
[28] Powder Diffraction File. Data Cards. Inorganic Section. Set 33, card 241. JCPDS, Swarthmore, PA, USA (1948).
[29] Powder Diffraction File. Data Cards. Inorganic Section. Set 33, card 240. JCPDS, Swarthmore, PA, USA (1948).
[30] Powder Diffraction File. Data Cards. Inorganic Section. Set 33, card 744. JCPDS, Swarthmore, PA, USA (1948).
[31] G.C. Vezzoli. Phys. Rev. B **26**, *7*, 3954 (1982). https://doi.org/10.1103/PhysRevB.26.3954
[32] L.A. Reznichenko, L.A. Shilkina, E.S. Gagarina, Y.I. Yuzyuk, O.N. Razumovskaya, A.V. Kozinkin. Crystallogr. Rep. **49**, *5*, 820 (2004). https://doi.org/10.1134/1.1803313

Translated by E.Ilinskaya